



Published in final edited form as:

Nanotoxicology. 2013 December ; 7: . doi:10.3109/17435390.2012.741726.

Quantification of quantum dot murine skin penetration with UVR barrier impairment

Luke J. Mortensen^{*}, Samreen Jatana^{*}, Robert Gelein[†], Anna De Benedetto[§], Karen L. De Mesy Bentley[‡], Lisa Beck[§], Alison Elder[†], and Lisa A. DeLouise^{*,§,1}

^{*}Department of Biomedical Engineering, Rochester, NY, 14642

[†]Department of Environmental Medicine, Rochester, NY, 14642

[§]Department of Dermatology, University of Rochester, Rochester, NY, 14642

[‡]Department of Pathology and Laboratory Medicine, Rochester, NY, 14642

Abstract

Ultraviolet radiation (UVR) skin exposure is a common exogenous insult that can alter skin barrier and immune functions. With the growing presence of nanoparticles (NPs) in consumer goods and technological applications the potential for NPs to contact UVR exposed skin is increasing. Therefore it is important to understand the effect of UVR on NP skin penetration and potential for systemic translocation. Previous studies qualitatively showed that UVR skin exposure can increase the penetration of NPs below the stratum corneum. In the present work, an *in vivo* mouse model was used to quantitatively examine the skin penetration of carboxylated (CdSe/ZnS, core/shell) quantum dots (QDs) through intact and UVR barrier disrupted murine skin by organ Cd mass analysis. Transepidermal water loss was used to measure the magnitude of the skin barrier defect as a function of dose and time post UVR exposure. QDs were applied to mice 3-4 days post UVR exposure at the peak of the skin barrier disruption. Our results reveal unexpected trends that suggest these negative charged QDs can penetrate barrier intact skin and that penetration and systemic transport depends on the QD application time post UVR exposure. The effect of UVR on skin resident dendritic cells and their role in the systemic translocation of these QDs are described. Our results suggest that NP skin penetration and translocation may depend on the specific barrier insult and the inflammatory status of the skin.

Keywords

Skin; Quantum dots; UVR; transepidermal water loss; Langerhans cells

1 Introduction

The expanding use of nanomaterials in consumer and technological applications has motivated studies to investigate the risks associated with human and environmental nanoparticle (NP) exposure (NNI, 2008; NIOSH, 2009). A primary human exposure route is the skin and therefore many studies have sought to elucidate factors that can impact NP skin penetration. Considerable work has focused on TiO₂ and ZnO NPs, which are commonly formulated into ultraviolet radiation (UVR) protective sunscreens and cosmetics products. Studies of barrier intact skin, employing numerous human and animal skin models,

¹To whom correspondence should be addressed at the Department of Dermatology, University of Rochester, Box 697, Rochester, NY, 14642. Phone: (585) 275-1810. Lisa_DeLouise@urmc.rochester.edu.

generally report no significant evidence for ZnO or TiO₂ NP penetration beyond the stratum corneum (Cross et al., 2007; Tan et al., 1996 ; Gamer et al., 2006; Schulz et al., 2002; Lademann et al., 1999; Mavon et al., 2007; Pflucker et al., 1999; Roberts et al., 2008; Schulz et al., 2002; Wu et al., 2009; Zvyagin et al., 2008). Much less is understood, however, about how UVR skin exposure may modulate the susceptibility to NP stratum corneum penetration and systemic transport.

It is well established that UVR skin exposure induces dose and time dependent biological responses including erythema, inside-out barrier dysfunction as measured by transepidermal water loss, and immunosuppression characterized by a depletion of skin resident dendritic cells (Abe & Mayuzumi, 1979). Interestingly, the combined effects of UVR induced immunosuppression and barrier dysfunction do not result in an increased incidence of skin microbial infections as UVR exposure also induces expression of antimicrobial peptides in skin (Glaser et al., 2009). How the impacts of UVR exposure on skin barrier and skin immune function may affect NP skin penetration and systemic transport are not yet understood.

One recent human subjects study investigated the effect of repeated (7 consecutive days) topical application of a sunscreen lotion containing ZnO NPs to UVR exposed skin and found significant increases of Zn ion levels in the blood and urine of volunteers, suggesting that UVR exposure may enhance penetration of NPs through human skin (Gulson et al. 2010). It was not however, determined in this study whether Zn ions or intact ZnO NPs penetrated the stratum corneum. Another study employing an *in vivo* pig model reported, based on analysis of transmission electron microscopy (TEM) images and diffusion cell measurements, that UVR exposure slightly enhanced the penetration of TiO₂ and ZnO NPs through layers in the stratum corneum (Monteiro-Riviere et al. 2011). The depth of penetration was found to depend on the formulation of the vehicle in which the NPs were topically applied. The above studies corroborate our findings reported earlier (Mortensen et al. 2008) that UVR exposure could enhance the penetration of quantum dot (QD) NPs though the stratum corneum and into the viable mouse epidermis.

QDs are fluorescent NPs that are increasingly being utilized in commercial and technological applications (Koleilat et al., 2008; Lee et al., 2010; Li et al., 2010; Wu et al., 2004). Therefore, understanding how QDs interact with skin is a primary concern. QDs are also powerful probes, with a distinct advantage over nonfluorescent NPs in their ability to be more easily tracked in tissues provided the signal can be detected above background autofluorescence (Mortensen et al., 2010; Mortensen et al., 2011). The qualitative findings discussed above suggest that UVR skin exposure induces an outside-in barrier defect that can increase the susceptibility of NPs to penetrate the stratum corneum. Quantitative studies of NP penetration through UVR exposed skin are lacking and warranted as the number of NP containing skin care products is on the rise (Nohynek et al., 2010) and UVR skin exposure is a common environmental insult. The present study seeks to quantify the effect of UVR skin exposure on the penetration of negatively charged QDs using the SKH-1 *in vivo* mouse model. We investigate the impact of UVR dose on skin barrier function and relate the peak of the barrier defect to the penetration of QDs using organ elemental analysis. Our results reveal unexpected trends that suggest QD skin penetration and systemic transport depend on UVR exposure and the QD application time post UVR exposure. The effect of UVR on skin resident dendritic cells and their role in QD systemic translocation are described.

2 Materials and Methods

2.1 Quantum Dot Functionalization and Vehicle Preparation

To prepare water-soluble QDs for use in this study, we purchased (NN-Labs, Fayetteville, Arkansas) spherical CdSe/ZnS core-shell QDs in organic solvent (toluene) with a peak emission wavelength of 620 nm. Water-soluble carboxylic acid coated QDs were generated by ligand exchange with dihydrolipoic acid (DHLA) as described previously (Mortensen et al., 2009). Briefly, a ~10,000× molar excess of pure DHLA to QDs is added to 1 mL methanol and the pH adjusted to 11.0-12.0 using tetramethylammonium hydroxide pentahydrate powder (Sigma-Aldrich Inc., St. Louis, Missouri). The QDs (250 μ L, 1.25 mg) were precipitated from toluene using excess methanol/acetone (50/50) and centrifugation at 14,000 rpm (~23000 g). They were then resuspended in tetrahydrofuran (THF) and added drop-wise to the DHLA reaction mixture. The reaction was incubated at 60°C with stirring for 3 hours, then overnight at room temperature. The QDs were mixed with excess ether to precipitate with centrifugation at 14,000 rpm for 10 min. The ether was poured off, the pellet dried with nitrogen gas, and the QDs resuspended in water. The QDs were dialyzed using a 5 kD molecular weight cutoff DispoDialyzer filter (Harvard Apparatus Inc., Holliston, Massachusetts) in 500× excess volume of water for 72 hours with water changes every 24 hours. After dialysis, the concentration was determined by measuring the absorption at the first exciton using Lambert-Beer's law and an extinction coefficient determined from the literature (Yu et al., 2003). To determine the physiochemical properties of our functionalized QDs we measured the hydrodynamic diameter and zeta potential at a concentration of ~10-20 nM in water and the *in vivo* application vehicle (described below) using a Malvern Instruments Zetasizer Nano ZS (Malvern Instruments Ltd, Worcestershire, United Kingdom).

2.2 UVR Irradiation and Transepidermal Water Loss

To examine barrier response by Transepidermal water loss (TEWL) and the skin penetration of QDs, we used hairless SKH-1 mice back-crossed onto the C57BL/6 mouse as described previously (Mortensen et al., 2008). These mice are unpigmented and immunocompetent. They exhibit normal skin function with the exception of developing alopecia after the first cycle of normal hair growth. Mice were allowed access to water and standard mouse feed ad libitum and housed under constant humidity and temperature with 1 mouse per cage and 12 hour light/dark cycles during UVR-irradiation and recovery experiments. All mouse experiments were performed on animals 8-10 weeks in age weighing 25-30 g. For the TEWL experiments, a designed experiment approach was utilized with a full factorial 64 treatment condition array including a 2-level gender factor (male and female), a 4-level ultraviolet B (UVB) dose factor (0 mJ/cm², 180 mJ/cm², 270 mJ/cm², and 360 mJ/cm²), and an 8-level day factor (0-7 days post-UVR exposure) with n=2. TEWL was measured using the Tewameter TM 300 with a mouse adaptor (Courage-Khazaka, Koln, Germany) with 60 seconds equilibration time to ensure consistent measurement. After equilibration, TEWL was measured once a second for 30 seconds and the values averaged to provide a single reading for each mouse. To minimize measurement variability the room temperature, the relative humidity, and the time of day were fixed. The TEWL was measured for 4 consecutive days to establish a baseline for each mouse. The mice were irradiated in a standard laboratory setting according to procedures detailed elsewhere (Mortensen et al., 2008). Briefly, mice were housed individually and exposed at a distance of 15 inches to UVA Sun 340 lamps, which emits across the UVA (320-400 nm) and UVB spectra (290-320 nm), closely resembling the UVR spectrum of sunshine (Tripp et al., 2003). Throughout the text we refer to UVR exposure but denote the specific UVB dose as the lamps were calibrated to UVB output using an IL1700 light meter (International Light) with a SED 240 probe (255-320 nm detection). The exposure time to achieve the desired UVB dose was

calculated using the measured flux value (J/cm^2 -sec). TEWL was then measured immediately after UVR exposure and each day subsequently for 7 days at the same time each day. A near equivalent UVB exposure of 180, 270, and 360 mJ/cm^2 would be achieved by spending 11, 16, and 22 min in the direct sun at noon time in mid-July in Rochester, NY.

2.3 UVR Irradiation and Langerhans Cell Density

To examine the effect of UVR on Langerhans cell density we exposed mice to 360 mJ/cm^2 UVB using the procedure described above. After 4 days post UVR exposure the mice were sacrificed humanely according to a protocol approved by the University Committee on Animal Resources (UCAR). Skin samples were harvested from the backs (5 cm^2 in area) of the UVR exposed and control (no UVR) mice. Skin samples were thinned from the dermis side using a scalpel and stained for Langerhans cells (LCs) using the following protocol. The thinned skin was fixed in methanol (15 minutes at 4 °C), blocked using 2% bovine serum albumin (BSA, HyClone, Cat. No. SH30574.01) for 30 minutes at room temperature. Next, the skin was treated with Fc Block (anti-CD16/CD32, eBioscience, Cat. No: 14-0161-82) diluted 1:100 in 2% BSA for 30 minutes at room temperature. Staining for LCs was achieved using anti-CD207 (eBioscience, Cat. No: 53-2073-82) diluted 1:100 in 2% BSA overnight at 4 °C. After washing x2 in PBS the stained samples were mounted with the epidermis facing down on glass bottom microwell dishes (MatTek Corporation). The samples were coated with mowiol and a cover slip was then placed on the dermis to flatten the sample for confocal imaging using a FV1000 Olympus Laser Scanning Confocal Microscope. The number densities of positively stained LCs in the epidermis were quantified using Image J software (NIH version 1.45).

2.4 QD Application to Mice

QDs or a vehicle control were applied to the backs of n=5 mice 3.5-4.5 days post-UVR exposure (0 mJ/cm^2 or 360 mJ/cm^2 UVB irradiation) when the TEWL value was near maximum using previously discussed techniques (Mortensen et al., 2008). Briefly, prior to application of the QD glycerol solution, each mouse was fitted with an Elizabethan collar (Braintree Scientific, Braintree, Massachusetts) to avoid removal from grooming and ingestion of the applied QDs. Each mouse was treated with 30 μL of 3.5 μM DHLA QDs in 30% glycerol over $\sim 6 cm^2$ area of their back, with the dose spread evenly over the skin with a 200 μL pipette tip. This provided a final QD dose of $\sim 17.5 pmol/cm^2$. The collars minimally affected mouse behavior, with a slightly more subdued activity level being the only observable impact. After 24 hrs of QD application the mice were sacrificed and their skin and organs harvested and treated for analysis as described below. All procedures were approved by the University Committee on Animal Research (UCAR).

2.5 Dissection and Organ Analysis

After sacrifice, excess QDs remaining on the skin surface were carefully wiped off using sterile 1 \times PBS soaked gauze and then dried. The UVR exposed and QD skin application area was harvested from the back and processed for immunohistochemistry and TEM analysis as described in Sections 2.6 and 2.7. Next, the proximal lymph nodes (axillary and brachial) and the liver were harvested from each animal and weighed. Organs were harvested using dedicated instruments, with the control animals (no QD) being dissected first. Between each animal, the dissection surface covering was changed and the instruments were cleaned and rinsed in H₂O then acetone, sonicated for 10 minutes in 1% HNO₃, and rinsed again to remove residual acid and to eliminate potential contaminants. The tissues were placed directly into pre-weighed digestion vials, weighed, and wet ashed with ultrapure 70% nitric acid (Baseline, SeaStar Chemicals Inc., Sidney, British Columbia, Canada). After nitric acid ashing, the tissue residue was resuspended in 2% HNO₃ diluted in 18 M deionized water before graphite furnace atomic absorption spectroscopy analysis.

Quantification was achieved through comparison to reference standards (Standard Reference Material 1577b from bovine liver; National Institute of Standards and Technology, Gaithersburg, MD). To ensure that experimental error did not contribute to the Cd signal found in the liver and lymph tissue for the 24 h QD exposure conditions, a 0 h QD exposure control was included. For this control, non-UVR irradiated animals had the standard concentration and volume of QDs applied to their backs, but they were immediately sacrificed and their organs collected for Cd level quantification using identical procedures described above. The amount of Cd in the applied dose was also quantified.

2.6 Skin Tissue Cryo-Processing

A portion of the skin was snap frozen using liquid nitrogen and stored at -80°C . These samples were later processed for analysis by mounting the skin in Tissue-TEK OCT (Sakura FineTek USA Inc. Torrance, CA). Skin was sectioned from dermal to epidermal side onto a microscope slide using a Microm HM 525 cryostat (Mikron Instruments, Inc. San Marcos, CA) at $10\ \mu\text{m}$ thickness, with the blade changed between slices. The blade precautions were taken to avoid accidental transfer of QDs from the skin surface to epidermal and dermal layers when slicing. After sectioning, all samples were fixed in 5% formalin in PBS for 10 minutes and mounted using Vectashield mounting media (Vector Laboratories, Inc.). The sections were imaged under a wide field fluorescence microscope (Olympus IX70 with QImaging Retiga EXL camera) with a mercury lamp excitation source (360/30 bandpass filter) and narrow emission (620/10 bandpass filter) and phase contrast microscopy to allow visualization of skin structures while minimizing autofluorescence in the QD fluorescence images.

2.7 Transmission Electron Microscopy

Transmission electron microscopy (TEM) was used to examine QD skin penetration at an ultrastructural level, namely their cellular localization. After 24 hour fixation in 2.5% glutaraldehyde, whole skin samples were postfixed in osmium tetroxide and silver enhanced using a standard AURION R-GENT SE-EM reagent and protocol as discussed previously (Mortensen et al., 2008). The silver enhancement selectively deposited on the QDs to allow them to be distinguished easily from the surrounding tissue (Chou et al., 2009). After silver enhancement, the skin samples were dehydrated using graded alcohol baths (25%, 50%, 75% and 100%) and then infiltrated with and embedded in Spurr epoxy resin with overnight polymerization at 70°C . After embedding, the samples were cut to $1\text{-}2\ \mu\text{m}$ with a glass blade and then sectioned at $70\ \text{nm}$ with a diamond knife and placed on copper grids. QD localization was evaluated using the Hitachi 5100 TEM apparatus with EDAX attachment to provide elemental analysis spectra of samples. To confirm that silver enhancement was optimized for contrast of QDs, samples were processed in an identical manner from vehicle only treated mice.

2.8 Statistical Analyses

A 3-way ANOVA was used to evaluate the impact of UVR dose, gender, and time on TEWL response with an $n=2$. Subsequent analyses were then done via a 2-way ANOVA after pooling by gender to yield $n=4$. Multiple group comparisons were done using unpaired Student's t-tests. For the analyses of organ Cd levels, 5 mice per group were used. Individual group comparisons of tissue Cd level were performed using unpaired Student's t-tests. For Langerhans cell studies a power analysis was performed on preliminary data with values $\alpha=0.01$, $\beta=0.05$, $(1-\beta)>0.95$. It was determined that $n=2$ mice were needed at each UVR dose (0 and $360\ \text{mJ}/\text{cm}^2$ UVB). We used age matched male and female mice for the Langerhans cell migration study. A unpaired Student's t-test was performed on individual groups for statistical comparisons.

3 Results

3.1 Transepidermal Water Loss

To investigate the effect of UVR on TEWL we first established individual baseline values for our outbred SKH-1 mice. To do so, we recorded the TEWL value for each mouse ($n=16$) on four consecutive days. Averaging the baseline values for all mice yielded a TEWL value of 4.15 ± 0.73 g/m²/h. Groups of mice ($n=4$) were then exposed to four different UVR doses (0, 180, 270, 360 mJ/cm² UVB). ANOVA demonstrated that TEWL was strongly impacted by the UVR dose and post-exposure time ($p < 0.0001$ for each). Gender was not found to have a significant effect on TEWL ($p=0.18$). Therefore, pooled data from male and female mice are shown in Figure 1, where the TEWL values are reported as a function of UVB dose and time. The y-axis represents the average normalized TEWL value calculated by taking the TEWL value measured on each mouse, dividing by its individual four day baseline value, then averaging results ($n=4$ mice per data point). The plots show that by day 3 post-irradiation a statistically significant increase in TEWL occurs for each of the UVR-exposed groups. Some scaliness and redness was observed on the backs of the mice exposed to 270 mJ/cm² and 360 mJ/cm² UVB by day 3. Measurements on mice in all groups were taken in this general area. The peak TEWL value depended on UVR dose and time. A peak value of 2.33 ± 0.26 fold over the control was attained for the 180 mJ/cm² UVB dose at 4 days post UVR exposure, a peak value of 6.07 ± 1.74 fold over control was attained for the 270 mJ/cm² UVB dose at 5 days post UVR exposure, and a peak value of 8.84 ± 0.96 fold over control was attained for the 360 mJ/cm² UVB dose at 6 days post UVR exposure.

3.2 QD Characterization

To characterize our functionalized QDs, the hydrodynamic particle size and zeta potential in both water and the glycerol application vehicle were measured. Using the Malvern Zetasizer, we determined the size of our DHLA 620 nm QDs to be similar in both deionized water and the 30% glycerol-containing vehicle (Figure 2). This suggests that the QDs diluted in water and glycerol maintain a similarly monodisperse condition, with particle size of 14-15 nm. A zeta potential value of approximately -45 mV obtained in deionized water indicates strongly functionalized QDs. A similar zeta potential value of approximately -40 mV in 30% glycerol suggest that QDs maintain their charge, with the small difference in zeta potential being attributable to the pH difference between the solutions as indicated. The charge stability and monodispersity of our DHLA functionalized QDs in the application vehicle that is similar to the pH of skin may help to maintain solution characteristics and dispersity under our experimental conditions (Prow et al., 2011).

3.3 Microscopy Evaluation of QD Skin Collection and Penetration

Phase contrast and fluorescent microscopy images of histological sections from mouse skin following QD application to control skin (no UVR) and skin 3.5 days post UVR (360 mJ/cm² UVB) exposure are shown in Figure 3. Relative to control skin (Figure 3A), there is an obvious thickening and disorganization of the UVR exposed skin (Figure 3C). Common QD collection sites on non-irradiated skin occur in the outer layers of the stratum corneum (Figure 3A), with some preferential collection in folds and defects of the skin surface, as well as along hair follicles (Figure 3B). In UVR irradiated skin, there is an increased presence of QDs below the stratum corneum away from hair follicles, a representative example of which is shown in Figure 3C. Similar collection trends were observed around the hair follicle, but with a more consistent depth of penetration (Figure 3D). It is important to note however, that by histological analysis the occurrences of QD penetration below the stratum corneum on UVR exposed skin were rare events. Most commonly, the occurrences were localized to areas that had obvious morphological damage and thickening of the stratum corneum. Furthermore, the occurrences of penetration in UVR exposed skin

appeared more commonly as QD clusters below the stratum corneum rather than as individual QDs.

3.4 Ultrastructural TEM Analysis of Penetration Pathways

TEM combined with silver enhancement to amplify the presence of QDs in skin sections was established in our previous work (Mortensen et al., 2008). Silver treatment increases the size and contrast of the QDs, thereby allowing their distinction from inherent tissue features. For the no UVR control, collection of QDs was primarily observed in the outer layers of the stratum corneum, with some collection in the hair follicles (Figure 4), which is consistent with the tissue histology. Some penetration through the outer layers of the stratum corneum could be observed (Figure 4A), with QDs appearing to move through the intercellular lamellar space as found in previous work (Mortensen et al., 2008). We were unable to find many instances of penetration of QDs past the stratum corneum barrier for the no UVR control mice. However, when considering the 360 mJ/cm² UVB samples, some distinct morphological and QD penetration differences were apparent (Figure 5). The stratum corneum of all samples is substantially thickened and the intercellular connections appear much looser. Nuclei and unprocessed lamellar granules are visible in a number of locations at the outer portions of the stratum corneum, which is a common feature of UVR damage and may contribute to barrier impairment (Jiang et al., 2006). Additionally, the number of cell layers between the bottom of the stratum corneum and the dermal/epidermal junction is higher with an overall increase in thickness. The differentiating keratinocytes throughout the epidermis appear to have looser junctions as well, and their shape and morphology are altered. Analysis of the UVR exposed mouse sections suggest that the QDs were able to make it further through the loosened outer layers of the stratum corneum intercellular space (Figure 5A). Some occurrences of corneocytes filled with large amounts of QDs were observed (Figure 5A,i). Analysis of many TEM sections suggest that isolated areas with relatively higher amounts of stratum corneum damage may allow less hindered penetration of QDs. Similar to the histological imaging (Figure 4), scarce but higher penetration levels through the stratum corneum were observable in UVR irradiated samples (Figure 5) compared to the no UVR control samples. Non-QD control skin samples exhibit very low levels of silver staining, suggesting that the noise floor for our TEM technique is very low (supplementary data). The small sampling area achievable with the TEM analysis technique is however, a strong limiting factor for accurate evaluation of the effect of UVR on QD skin penetration.

3.5 Quantitative Distal Organ Analysis

Histological and TEM analysis provide important insight into the localization of QDs in the skin and some understanding of penetration mechanism, but they do not yield quantitative information. To evaluate the impact of UVR on skin penetration of QDs at a systemic level, it is necessary to look at organ collection patterns. We used atomic absorption spectroscopy to quantify Cd presence in the lymph nodes and livers of mice as a function of UVR (360 mJ/cm²) exposure and QD application. Calibration studies found that the Cd limit of detection (LOD) was 0.033 ng/ml and the limit of quantification (LOQ) was 0.111 ng/ml. The total QD dose applied to mice (glycerol vehicle plus QD) weighed 0.033 g (6 cm² area), and was calculated to contain 105.0 picomoles of QDs. Elemental analysis of the dose applied was found to contain 112.7±1.7 µg Cd. The total liver and lymph node organ Cd (ng) is shown in Table 1, and the tissue distribution (ng/g) is shown in Figure 6. Results indicate the presence of a baseline Cd level in the livers of control mice (vehicle treatment only). The likely source of this Cd is from their food. Application of QDs to control mice (no UVR) did not increase the liver Cd level. However, application of QDs to UVR exposure (360 mJ/cm² UVB) skin did show a statistically significant increase in liver Cd compared to the non-irradiated vehicle treated and non-irradiated QD treated mice (p<0.05).

The increase above background was however low, accounting for 0.0035% of the applied QD dose. Elemental analysis of the lymph nodes in control mice (vehicle treatment only) found unquantifiable baseline Cd levels (below the limit of quantification, LOQ) with and without UVR exposure. Application of QDs to UVR exposed skin elevated the Cd levels in lymph nodes of mice, 0.57 ± 0.10 ng (25.12 ± 7.29 ng/g). Unexpectedly, we also detected Cd in the lymph nodes of the control (no UVR) mice, 1.03 ± 0.08 ng (64.13 ± 11.28 ng/g). These values equate to 0.0005% and 0.0012% of the applied dose, respectively. To confirm that the detection of Cd in the lymph nodes of QD exposed control mice (no UVR) was not due to contamination, an additional control was performed with QD application to control skin (no UVR) followed by immediate sacrifice (i.e. ~0 hr exposure). This control found Cd levels below the LOQ in the lymph nodes indicating that the presence of Cd in the lymph nodes of mice treated with QD (no UVR) for 24 hr did not result from technique error but rather from systemic transport that occurred over the time period of the experiment. These findings suggest that QDs can penetrate barrier intact mouse skin and that UVR (360 mJ/cm² UVB) exposure decreases transport to the lymph node. While penetration of QDs through control skin (no UVR) is not suggested by liver Cd analysis, tissue histology or TEM, it is plausible that the low levels of penetration observed made it difficult to detect Cd above background levels. QD presence could also be missed on tissue sectioning or difficult to detect above tissue autofluorescence. UVR exposed mice did however, exhibit a statistically significant increase in liver Cd over baseline confirming QD skin penetration and systemic translocation. The decreased Cd level in the lymph node of UVR exposed mice suggests an effect of UVR on the mechanism of systemic transport which we explore in the next section.

3.6 Effect of UVR on Langerhans Cell Density

Skin resident antigen presenting dendritic cells, in particular Langerhans cells (LCs), have been shown to play critical roles in skin immunity and in the development of UVB-induced immunosuppression (Schwarz et al. 2010). Under skin inflammatory conditions or following UVR exposure, LCs migrate from the skin to the local lymph nodes to activate appropriate T cell populations (Schwarz et al. 2010; Kissenpfenning et al. 2005). A recent study of cutaneous vaccination showed that nanoparticles loaded with DNA were uptaken by LCs in the epidermis and they migrated to the draining lymph node where encoded gene products were expressed (Lee et al. 2010). Hence, the ability of LCs to uptake NPs in skin combined with the effect of UVR induced LC migration to the lymph nodes suggests a plausible mechanism for the detection of lower Cd levels in the UVR exposed mice relative to control (no UVB) reported above. To support this we used confocal microscopy to quantify the LC density in the skin of control mice (no UVR) and in mice four days post UVR exposure (360 mJ/cm² UVB), the approximate time when the TEWL barrier defect was at a maximum and when the QDs were applied. Results find that UVR exposure significantly depleted (~80%) the LCs in the skin at day 4 relative to the control (Figure 7). The average density in control skin is 478 LCs/mm², and this decreases to 79 LCs/mm² 4 days post UVR exposure. The presence of fewer LCs in the skin at the time of QD application suggests a reduced capacity to traffic QDs to the lymph node which is consistent with the lower Cd level measured in the lymph node of the UVR exposed mice relative to the control.

4 Discussion

The skin has had an increasing amount of research effort focused on determining the ability of NPs to penetrate the intact and damaged skin barrier. We report herein a low-level skin penetration of (CdSe/ZnS, core/shell) DLHA coated QDs through intact and UVR barrier disrupted murine skin qualitatively examined by histological and TEM analysis and quantitatively examined by organ Cd mass analysis. TEWL was used to measure the

magnitude of the UVR induced skin barrier defect. The TEWL time course and UVB dose results agree well with previous trends reported in the SKH-1 mouse model that were measured at much lower UVB doses ($<150 \text{ mJ/cm}^2$) than investigated in this study (Haratake et al., 1997; Haratake et al., 1997; Holleran et al., 1997; Jiang et al., 2006; Jiang et al., 2007). The UVR induced inside-out water loss defect is thought to be due to a combination of proliferation and immunologic responses that alter the epidermal calcium gradient (Jiang et al., 2007) and status of lipids in the stratum corneum (Jiang et al., 2006). With regard to the penetration of substances applied to UVR exposed skin, the only other study relating TEWL and outside-in skin permeation that we are aware investigated the skin penetration of ^{14}C -labeled hydrocortisone using a rat model (Lamaud & Schalla, 1984). Clear evidence was found for an increase in hydrocortisone skin penetration that corresponded with the increased UVR induced TEWL value observed. Our results also suggest a positive correlation of inside-out TEWL value and increased outside-in QD skin penetration as measured by tissue histology, TEM, and Cd mass in the liver of mice. However, since skin permeability and translocation may depend on injury severity and the specific barrier disrupting agent (Tsai et al., 2003; Tsai et al., 2001), further research is required to quantify the extent of the correlation between TEWL value and NP outside-in penetration as well as to conduct studies to estimate differences in penetration levels in human skin which is thicker than mouse skin.

Enhanced NP penetration through barrier defective skin is a common finding (Gopee et al., 2009; Kuo et al., 2009; Lopez et al., 2011; Mortensen et al., 2008; Mortensen et al., 2009; Paliwal et al., 2006; Prow et al. 2011; Ravichandran et al., 2010; Seto et al., 2010; Zhang & Monteiro-Riviere, 2008). The histological and TEM results presented in this study suggest the presence of isolated instances of high fluency entry points where localized weaknesses in the barrier allow QDs to penetrate. These locations have been described by Paliwal et al. as lacunar pathways, and their role has been identified in studies investigating the impact of ultrasound on QD skin penetration (Paliwal et al., 2006). Low frequency entry points can be expanded by certain forms of barrier disruption as was shown in studies investigating the effect of chemical penetration enhancers on ZnO NP skin penetration (Kuo et al., 2009). Lacunar pathways are also found in healthy skin but because of their lower frequency they can be easily missed on tissue histology or TEM. The histological analysis in this work was performed on 20-30 sections for each treatment condition, which equates to the examination of $0.02\text{-}0.03 \text{ cm}^2$ of skin surface, or $\sim 0.3\text{-}0.5\%$ of the application area. The lacunar imperfections postulated by Paliwal et al. were described as being approximately 48 nm in diameter and covering 0.44% of the skin surface area (Paliwal et al., 2006). Therefore, many sections must be examined to find evidence of such permeation. Combined with the difficulty to distinguish individual visible emitting QDs (620 nm) above background tissue autofluorescence (Mortensen et al., 2010; Mortensen et al., 2011) it is not surprising that detection of penetration through intact skin was missed on histology. Analysis of 70 nm thick TEM sections examines considerable less of a % of the application area thereby making it even more difficult to observe scarce events. Hence, lacunar pathways in control skin may be a contributing source of the Cd detected in the lymph nodes of the control mice. A similar conclusion was postulated by Lopez et al. to explain the observed penetration of QDs into the dermis of pig skin (Lopez et al., 2011). Our observations suggesting that QDs can penetrate through intact mouse skin is supported by literature. QDs with positive, negative, and neutral surface coatings and hydrodynamic diameters ranging from 10-22 nm were reported to penetrate healthy split thickness *ex vivo* porcine skin in low amounts (Lopez et al., 2011; Seto et al., 2010). Sonavane et al. reported that 15 nm diameter Au particles penetrated *ex vivo* rat skin (Sonavane et al. 2008) and Huang et al. reported that 5 nm Au NP could diffuse through intact mouse skin (Huang et al. 2010).

While there are numerous qualitative studies of NP stratum corneum penetration, only a few have attempted to quantify NP skin and systemic translocation. One important study by Gopee et al. quantified the skin penetration of PEG-ylated nail-shaped QDs with a 40 nm hydrodynamic diameter using the *in vivo* SKH-1 hairless mouse model (Gopee et al., 2009). They reported the highest presence of Cd in the liver and the regional draining lymph nodes (axillary and brachial) for QDs applied to dermabraded skin, which motivated our focus on these organs in this study. Dermal abrasion is an invasive technique that eliminates the stratum corneum and much of the epidermis to allow free access of QDs to the dermis and vasculature. This treatment resulted in a liver Cd level of ~2% of the applied dose (~211 ng Cd) (Gopee et al., 2009). In contrast, our UVR treatment induced a much weaker barrier defect that slightly increased the liver Cd above background corresponding to ~0.0035 % of the applied dose (~4 ng above background). They did not detect Cd in the lymph nodes when QDs were applied to barrier intact control skin, which is in contrast to our findings. It is possible that their usage of nail-shaped QDs with a larger hydrodynamic radius and PEG surface coating may have altered stratum corneum penetration or the transport mechanism to the lymph nodes. PEG ligand is a stealth surface coating that is well known to alter the organ collection and cell uptake of NPs in the body (Akerman et al., 2002; Schipper et al., 2009). It is important to note that the elemental analysis methods used in this and the Gopee (Gopee et al., 2009) study to quantify QD skin penetration do not distinguish between particulate and ionic systemic transport. Elemental quantification of Se and stoichiometric comparison to Cd would still be insufficient to draw conclusions about the form of QD material transported as the body processes Se (an essential element) differently than Cd (a heavy metal toxin) (Wahba et al., 1993; Skowerski et al., 2000; Kotyzová et al. 2010). Confirmatory particulate QD transport could be made by detection of QD fluorescence in distal organs which is currently being investigated.

The intriguing observation of this study is that the application of QD to UVR exposed mice, while causing elevated Cd liver levels, resulted in a ~45% lower Cd level in the lymph nodes compared to control skin (no UVR). This suggests a strong impact of UVR on QD skin penetration and a possible role for immune cell mediated translocation of QD to lymph nodes. Langerhans cells are the major epidermal antigen presenting cell type in skin (Randolph et al., 2005; Ruedl et al., 2000) and they have been shown to uptake polymer NPs topically applied to skin and traffic them to the lymph nodes (Vogt et al., 2006; Lee et al. 2010). It is well known that UVR exposure is immunosuppressive, inducing LCs emigration to the lymph nodes. This process occurs immediately after UVR exposure and lasts for 4-14 days (Aberer et al., 1981; Stingl et al., 1981; Toews et al., 1980). The lower Cd level measured in the lymph nodes of UVR exposed mice, relative to the control, is consistent with the fact that QD were applied 3.5 days post UVR exposure; a time point that we showed the LCs are depleted by ~80% in the epidermis. Studies are currently underway to validate this mechanism by detecting and quantifying the presence of QDs in LCs in skin and in the lymph nodes as a function of UVR exposure and time. In addition, we are mapping the kinetics of UVR induced LCs migration in our specific mouse model and we plan to quantify the QD systemic transport as a function of UVR dose and QD application time post UVR exposure. Because the quantitative elemental mass analysis technique used here cannot distinguish between transport of soluble Cd ion or QD nanoparticle transport, the observation of QD fluorescence in the lymph node will help confirm the proposed active cellular QD transport mechanism. The data presented here, nevertheless, suggests that the systemic transport of QDs, and perhaps all NP types that penetrate skin, may depend on the specific barrier insult and the inflammatory status of the skin.

5 Conclusions

In conclusion, we have demonstrated that UVR irradiation significantly impacts skin barrier function and the permeation and systemic trafficking of topically applied DLHA coated QDs. Penetration of QDs through barrier intact control skin was difficult to detect by fluorescence microscopy analysis of tissue sections and TEM. However, a statistically significant elevated level of Cd was detected in the lymph nodes of control animals (no UVR) to which QD were applied suggesting that penetration may occur through low frequency defects (lacunar pathways) in the stratum corneum. UVR exposure induced a substantial thickening of the epidermis and an apparent loosening of intercellular connections between epidermal cells. We observed a time and UVR dose dependent increase in TEWL value and a more substantial penetration of QDs based on histological and TEM analysis of tissue sections. Application of QDs to UVR exposed (360 mJ/cm² UVB) mice resulted in a statistically significant increase in liver Cd. Presumably QDs are transported to the liver via the circulatory system which they can access in the vascularized dermis. Interestingly, relative to control mice (no UVR) a statistically significant lower Cd level in the lymph node was measured in UVR (360 mJ/cm² UVB) exposed mice to which QD were applied. This result suggests that trafficking of QDs to the lymph node depends on the presence of Langerhans cells in the epidermis as QDs were applied to skin at a time point post UVR exposure where the Langerhans cell density was significantly (80%) depleted. The results reported here-in have heightened awareness about NP skin permeation and the possible dependence of systemic trafficking on barrier disruption type and skin immune status. To more fully characterize this phenomenon our on-going research is focused on conducting dose and time-course studies for the combination of UVR and QDs. We seek to quantify the effect of UVR on Langerhans cells migration and trafficking of QD nanoparticles from skin to the lymph nodes as a function of UVB dose and time post UVR exposure. Mechanistic insight into how NP may affect Langerhans cell trafficking and/or antigen presentation are important for assessing risk from NP skin exposure but also for optimizing NP based transdermal drug or vaccine delivery.

Supplementary Material

Refer to Web version on PubMed Central for supplementary material.

Acknowledgments

We would like to thank Karen Vanderbilt for cryo-histology sectioning, Gayle Schneider for TEM processing assistance and Linda Callahan for assistance with confocal imaging. This publication was made possible by Grant Number UL1 RR024160 from the National Center for Research Resources (NCRR), a component of the National Institutes of Health (NIH), and the NIH Roadmap for Medical Research. This work was also supported by the National Science Foundation (CBET 0837891), the National Institute of Health (NIAID K25AI060884), and the National Institute of Environmental Health Sciences (ES01247).

References

- Abe T, Mayuzumi J. The change and recovery of human skin barrier functions after ultraviolet light radiation. *Chem Pharm Bulletin*. 1979; 27:458–462.
- Aberer W, Schuler G, Stingl G, Hönigsmann H, Wolff K. Ultraviolet light depletes surface markers of Langerhans cells. *J Invest Dermatol*. 1981; 76:202–210. [PubMed: 6453905]
- Akerman ME, Chan WC, Laakkonen P, Bhatia SN, Ruoslahti E. Nanocrystal targeting in vivo. *Proc Natl Acad Sci U S A*. 2002; 99(20):12617–12621. [PubMed: 12235356]
- Alvarez-Román R, Naik A, Kalia YN, Guy RH, Fessi H. Skin penetration and distribution of polymeric nanoparticles. *J Control Release*. 2004; 99:53–62. [PubMed: 15342180]

- Baroli B, Ennas MG, Loffredo F, Isola M, Pinna R, López-Quintela MA. Penetration of metallic nanoparticles in human full-thickness skin. *J Invest Dermatol.* 2007; 127:1701–1712. [PubMed: 17380118]
- Black AK, Fincham N, Greaves MW, Hensby CN. Time course changes in levels of arachidonic acid and prostaglandins D2, E2, F2 alpha in human skin following ultraviolet B irradiation. *Br J Clin Pharmacol.* 1980; 10:453–457. [PubMed: 7437257]
- Chou LYT, Fischer HC, Perrault SD, Chan WCW. Visualizing Quantum Dots in Biological Samples Using Silver Staining. *Anal Chem.* 2009; 81:4560–4565. [PubMed: 19408951]
- Cross SE, Innes B, Roberts MS, Tsuzuki T, Robertson TA, McCormick P. Human skin penetration of sunscreen nanoparticles: In-vitro assessment of a novel micronized zinc oxide formulation. *Skin Pharmacol Appl Skin Physiol.* 2007; 20:148–154.
- Dabbousi BO, Rodriguez-Viejo J, Mikulec FV, Mattoussi H, Ober R, Jensen KF, Bawendi MG. CdSe)ZnS core-shell quantum dots: synthesis and characterization of a size series of highly luminescent nanocrystallites. *J Phys Chem B.* 1997; 101:9463–9475.
- Endo K, Suzuki N, Yoshida O, Sato H, Fujihura Y. The barrier component and the driving force component of transepidermal water loss and their application to skin irritant tests. *Skin Res Technol.* 2007; 13:425–435. [PubMed: 17908195]
- Epstein JH, Fukuyama K, Fye K. Effects of ultraviolet radiation on the mitotic cycle and DNA, RNA and protein synthesis in mammalian epidermis in vivo. *Photochem Photobiol.* 1970; 12:57–65. [PubMed: 5498527]
- Gamer AO, Leibold E, van Ravenzwaay B. The in vitro absorption of microfine zinc oxide and titanium dioxide through porcine skin. *Toxicol In Vitro.* 2006; 20:301–307. [PubMed: 16182508]
- Gläser R, Navid F, Schuller W, Jantschitsch C, Harder J, Schröder JM, Schwarz A, Schwarz T. UV-B radiation induces the expression of antimicrobial peptides in human keratinocytes in vitro and in vivo. *J Allergy Clin Immunol.* 2009; 123(5):1117–23.
- Gopee NV, Roberts DW, Webb P, Cozart CR, Siitonen PH, Latendresse JR, Warbitton AR, Yu WW, Colvin VL, Walker NJ, Howard PC. Quantitative determination of skin penetration of PEG-coated CdSe quantum dots in dermabrased but not intact SKH-1 hairless mouse skin. *Toxicol Sci.* 2009; 111:37–48. [PubMed: 19574408]
- Gopee NV, Roberts DW, Webb P, Cozart CR, Siitonen PH, Warbitton AR, Yu WW, Colvin VL, Walker NJ, Howard PC. Migration of intradermally injected quantum dots to sentinel organs in mice. *Toxicol Sci.* 2007; 98:249–257. [PubMed: 17404394]
- Gulson B, McCall M, Korsch M, Gomez L, Casey P, Oytam Y, Taylor A, McCulloch M, Trotter J, Kinsley L, Greenoak G. Small amounts of zinc from zinc oxide particles in sunscreens applied outdoors are absorbed through human skin. *Toxicol. Sci.* 2010; 118:140–149. [PubMed: 20705894]
- Haratake A, Uchida Y, Schmuth M, Tanno O, Yasuda R, Epstein J, Elias P, Holleran W. UVB-induced alterations in permeability barrier function: roles for epidermal hyperproliferation and thymocyte-mediated response. *J Invest Dermatol.* 1997; 108:769–773. [PubMed: 9129231]
- Hardman R. A Toxicological Review of Quantum Dots: Toxicity Depends on Physico-Chemical and Environmental Factors. *Environ Health Persp.* 2006; 114:165–172.
- Holleran WM, Uchida Y, Halkier-Sorensen L, Haratake A, Hara M, Epstein JH, Elias PM. Structural and biochemical basis for the UVB-induced alterations in epidermal barrier function. *Photodermatol Photoimmunol Photomed.* 1997; 13:117–128. [PubMed: 9453079]
- Huang Y, Yu F, Park YS, Wang J, Shin MC, Chung HS, Yang VC. Coadministration of protein drugs with gold nanoparticles to enable percutaneous delivery. *Biomaterials.* 2010; 31:9086–9091. [PubMed: 20828812]
- Jeong SH, Kim JH, Yi SM, Lee JP, Kim JH, Sohn KH, Park KL, Kim MK, Son SW. Assessment of penetration of quantum dots through in vitro and in vivo human skin using the human skin equivalent model and the tape stripping method. *Biochem Biophys Res Commun.* 2010; 394:612–615. [PubMed: 20214881]
- Jiang SJ, Chen JY, Lu ZF, Yao J, Che DF, Zhou XJ. Biophysical and morphological changes in the stratum corneum lipids induced by UVB irradiation. *J Dermatol Sci.* 2006; 44:29–36. [PubMed: 16842978]

- Jiang SJ, Chu AW, Lu ZF, Pan MH, Che DF, Zhou XJ. Ultraviolet B-induced alterations of the skin barrier and epidermal calcium gradient. *Exp Dermatol*. 2007; 16:985–992. [PubMed: 18031457]
- Kissenpfennig A, Henri S, Dubois B, Laplace-Builhé C, Perrin P, Romani N, Tripp CH, Douillard P, Leserman L, Kaiserlian D, Saeland S, Davoust J, Malissen B. Dynamics and function of Langerhans cells in vivo: dermal dendritic cells colonize lymph node areas distinct from slower migrating Langerhans cells. *Immunity*. 2005; 22:643–654. [PubMed: 15894281]
- Koleilat GI, Levina L, Shukla H, Myrskog SH, Hinds S, Pattantyus-Abraham AG, Sargent EH. Efficient, stable infrared photovoltaics based on solution-cast colloidal quantum dots. *ACS Nano*. 2008; 2:833–840. [PubMed: 19206479]
- Kolgen W, Both H, van Weelden H, Guikers KL, Bruijnzeel-Koomen CA, Knol EF, van Vloten WA, De Gruijl FR. Epidermal Langerhans cell depletion after artificial ultraviolet B irradiation of human skin in vivo: apoptosis versus migration. *J Invest Dermatol*. 2002; 118:812–817. [PubMed: 11982758]
- Kotyzová D, Cerná P, Lesetický L, Eybl V. Trace elements status in selenium-deficient rats-Interaction with cadmium. *Biol Trace Elem Res*. 2010; 136:287–293. [PubMed: 19823775]
- Kuo T-R, Wu C-L, Hsu C-T, Lo W, Chiang S-J, Lin S-J, Dong C-Y, Chen C-C. Chemical enhancer induced changes in the mechanisms of transdermal delivery of zinc oxide nanoparticles. *Biomaterials*. 2009; 30:3002–3008. [PubMed: 19232716]
- Kupper TS, Chua AO, Flood P, McGuire J, Gubler U. Interleukin 1 gene expression in cultured human keratinocytes is augmented by ultraviolet irradiation. *J Clin Invest*. 1987; 80:430–436. [PubMed: 3497177]
- Lademann J, Weigmann H-J, Rickmeyer C, Barthelmes H, Schaefer H, Mueller G, Sterry W. Penetration of titanium dioxide microparticles in a sunscreen formulation into the horny layer and the follicular orifice. *Skin Pharmacol Appl Skin Physiol*. 1999; 12:247–256. [PubMed: 10461093]
- Lamaud E, Schalla W. Influence of UV irradiation on penetration of hydrocortisone. In vivo study in hairless rat skin. *British J Dermatol*. 1984; 111:152–157.
- Larese FF, D'Agostin F, Crosera M, Adami G, Renzi N, Bovenzi M, Maina G. Human skin penetration of silver nanoparticles through intact and damaged skin. *Toxicology*. 2009; 255:33–7. [PubMed: 18973786]
- Lee PW, Hsu SH, Tsai JS, Chen FR, Huang PJ, Ke CJ, Liao ZX, Hsiao CW, Lin HJ, Sung HW. Multifunctional core-shell polymeric nanoparticles for transdermal DNA delivery and epidermal Langerhans cells tracking. *Biomaterials*. 2010; 31:2425–2434. [PubMed: 20034662]
- Lewinski NA, Colvin VL, Drezek RA. Cytotoxicity of nanoparticles. *Small*. 2008; 4:26–49. [PubMed: 18165959]
- Li Z, Huang P, Lin J, He R, Liu B, Zhang X, Yang S, Xi P, Zhang X, Ren Q, Cui D. Arginine-glycine-aspartic acid-conjugated dendrimer-modified quantum dots for targeting and imaging melanoma. *J Nanosci Nanotechnol*. 2010; 10:4859–4867. [PubMed: 21125820]
- Lopez RF, Seto JE, Blankschtein D, Langer R. Enhancing the transdermal delivery of rigid nanoparticles using the simultaneous application of ultrasound and sodium lauryl sulfate. *Biomaterials*. 2011; 32:933–941. [PubMed: 20971504]
- Mavon A, Miquel C, Lejeune O, Payre B, Moretto P. In vitro percutaneous absorption and in vivo stratum corneum distribution of an organic and a mineral sunscreen. *Skin Pharmacol Applied Skin Physiol*. 2007; 20:10–20.
- Monteiro-Riviere NA, Wiench K, Landsiedel R, Schulte S, Inman AO, Riviere JE. Safety evaluation of sunscreen formulations containing titanium dioxide and zinc oxide nanoparticles in UVB sunburned skin: an in vitro and in vivo study. *Toxicol Sci*. 2011; 123(1):264–80. [PubMed: 21642632]
- Moritake S, Taira S, Ichihayashi Y, Morone N, Song SY, Hatanaka T, Yuasa S, Setou M. Functionalized nano-magnetic particles for an in vivo delivery system. *J Nanosci Nanotechnol*. 2007; 7:937–944. [PubMed: 17450856]
- Mortensen LJ, Oberdorster G, Pentland AP, DeLouise LA. In vivo skin penetration of quantum dot nanoparticles in the murine model: the effect of UVR. *Nano Lett*. 2008; 8:2779–2787. [PubMed: 18687009]

- Mortensen LJ, Zheng H, Faulknor R, De Benedetto A, Beck L, DeLouise LA. Increased in vivo skin penetration of quantum dots with UVR and in vitro quantum dot cytotoxicity. *Proceedings SPIE*. 2009; 7189:718919.
- Mortensen LJ, Ravichandran S, Zheng H, DeLouise LA. Progress and challenges in quantifying skin permeability to nanoparticles using a quantum dot model. *J Biomed Nanotechnol*. 2010; 6:596–604. [PubMed: 21329052]
- Mortensen LJ, Glazowski CE, Zavislan JM, DeLouise LA. Near-IR fluorescence and reflectance confocal microscopy for imaging of quantum dots in mammalian skin. *Biomedical Optics Express Biomed Opt Express*. 2011; 2(6):1610–1625.
- Approaches to Safe Nanotechnology Managing the Health and Safety Concerns Associated with Engineered Nanomaterials. NIOSH Publication No. 2009-125 available at: <http://www.cdc.gov/niosh/topics/nanotech/>
- Nohynek GJ, Antignac E, Re T, Toutain H. Safety assessment of personal care products/cosmetics and their ingredients. *Toxicol Appl Pharmacol*. 2010; 243(2):239–259. [PubMed: 20005888]
- NNI. Strategy for Nanotechnology-related environmental, health, and safety research. 2008. Available at : http://www.ostp.gov/galleries/NSTC/NNI_EHS_Research_Strategy.pdf
- Paliwal S, Menon GK, Mitragotri S. Low-frequency sonophoresis: ultrastructural basis for stratum corneum permeability assessed using quantum dots. *J Invest Dermatol*. 2006; 126:1095–1101. [PubMed: 16528354]
- Pentland AP, Scott G, VanBuskirk J, Tanck C, LaRossa G, Brouxhon S. Cyclooxygenase-1 deletion enhances apoptosis but does not protect against ultraviolet light-induced tumors. *Cancer Res*. 2004; 64:5587–5591. [PubMed: 15313895]
- Pflucker F, Hohenberg H, Holzle E, Will T, Pfeiffer S, Wepf R, Diembeck W, Wenck H, Gers-Barlag H. The outermost stratum corneum is an effective barrier against dermal uptake of topically applied micronized titanium dioxide. *Int J Cosmetic Sci*. 1999; 21:399–411.
- Prow TW, Monteiro-Riviere NA, Inman AO, Grice JE, Chen X, Zhao X, Sanchez WH, Gierden A, Kendall MA, Zvyagin AV, Erdmann D, Riviere JE, Roberts MS. Quantum dot penetration into viable human skin. *Nanotoxicology*. Apr 1.2011
- Prow TW, Grice JE, Lin LL, Faye R, Butler M, Becker W, Wurm EM, Yoong C, Robertson TA, Soyer HP, Roberts MS. Nanoparticles and microparticles for skin drug delivery. *Adv Drug Deliv Rev*. 2011a; 63(6):470–91. [PubMed: 21315122]
- Randolph GJ, Angeli V, Swartz MA. Dendritic-cell trafficking to lymph nodes through lymphatic vessels. *Nat Rev Immunol*. 2005; 5:617–628. [PubMed: 16056255]
- Ravichandran S, Mortensen LJ, DeLouise LA. Quantification of human skin barrier function and susceptibility to quantum dot skin penetration. *Nanotoxicology*. 2010 Early Online, 1-12.
- Roberts MS, Roberts MJ, Robertson TA, Sanchez W, Thörling C, Zou Y, Zhao X, Becker W, Zvyagin AV. In vitro and in vivo imaging of xenobiotic transport in human skin and in the rat liver. *J Biophotonics*. 2008; 1:478–493. [PubMed: 19343674]
- Rosado C, Pinto P, Rodrigues LM. Modeling TEWL-desorption curves: a new practical approach for the quantitative in vivo assessment of skin barrier. *Exp Dermatol*. 2005; 14:386–390. [PubMed: 15854133]
- Ruedl C, Koebel P, Bachmann M, Hess M, Karjalainen K. Anatomical origin of dendritic cells determines their life span in peripheral lymph nodes. *J Immunol*. 2000; 165:4910–4916. [PubMed: 11046016]
- Ryman-Rasmussen JP, Riviere JE, Monteiro-Riviere NA. Penetration of intact skin by quantum dots with diverse physicochemical properties. *Toxicol Sci*. 2006; 91:159–165. [PubMed: 16443688]
- Rzagalinski BA, Strobl JS. Cadmium-containing nanoparticles: perspectives on pharmacology and toxicology of quantum dots. *Toxicol Appl Pharm*. 2009; 238:280–288.
- Schwarz A, Noordegraaf M, Maeda A, Torii K, Clausen BE, Schwarz T. Langerhans cells are required for UVR-induced immunosuppression. *J Invest Dermatol*. 2010; 130:1419–1427. [PubMed: 20090769]
- Schipper ML, Iyer G, Koh AL, Cheng Z, Ebenstein Y, Aharoni A, Keren S, Bentolila LA, Li J, Rao J, Chen X, Banin U, Wu AM, Sinclair R, Weiss S, Gambhir SS. Particle size, surface coating, and

- PEGylation influence the biodistribution of quantum dots in living mice. *Small*. 2009; 5:126–134. [PubMed: 19051182]
- Schulz J, Hohenberg H, Pflücker F, Gärtner E, Will T, Pfeiffer S, Wepf R, Wendel V, Gers-Barlag H, Wittern K-P. Distribution of sunscreens on skin. *Adv Drug Deliv Rev*. 2002; 54(Suppl 1):S157–63. [PubMed: 12460721]
- Seto JE, Polat BE, Lopez RFV, Blankschtein D, Langer R. Effects of ultrasound and sodium lauryl sulfate on the transdermal delivery of hydrophilic permeants: comparative in vitro studies with full-thickness and split-thickness pig and human skin. *J Control Release*. 2010; 145:26–32. [PubMed: 20346994]
- Skowerski M, Jasik K, Konecki J. Effects of interaction between cadmium and selenium on heart metabolism in mice: the study of RNA, protein, ANP synthesis activities and ultrastructure in mouse heart. *Med Sci Monit*. 2000; 6(2):258–265. [PubMed: 11208320]
- Sonavane G, Tomoda K, Sano A, Ohshima H, Terada H, Makino K. In vitro permeation of gold nanoparticles through rat skin and rat intestine: effect of particle size. *Colloids Surf B Biointerfaces*. 2008; 65(1):1–10. [PubMed: 18499408]
- Stingl G, Gazze-Stingl LA, Aberer W, Wolff K. Antigen presentation by murine epidermal langerhans cells and its alteration by ultraviolet B light. *J Immunol*. 1981; 127:1707–1713. [PubMed: 6168700]
- Tan M-H, Commens CA, Burnett L, Snitch PJ. A pilot study on the percutaneous absorption of microfine titanium dioxide from sunscreens. *Australian J Dermatol*. 1996; 37:185–187.
- Tinkle SS, Antonini JM, Rich BA, Roberts JR, Salmen R, DePree K, Adkins EJ. Skin as a route of exposure and sensitization in chronic beryllium disease. *Environ Health Persp*. 2003; 111:1202–1208.
- Toews GB, Bergstresser PR, Streilein JW. Epidermal Langerhans cell density determines whether contact hypersensitivity or unresponsiveness follows skin painting with DNFB. *J Immunol*. 1980; 124:445–453. [PubMed: 6153101]
- Tripp CS, Blomme EA, Chinn KS, Hardy MM, LaCelle P, Pentland AP. Epidermal COX-2 induction following ultraviolet irradiation: suggested mechanism for the role of COX-2 inhibition in photoprotection. *J Invest Dermatol*. 2003; 121(4):853–861. [PubMed: 14632205]
- Tsai J-C, Shen L-C, Sheu H-M, Lu C-C. Tape stripping and sodium dodecyl sulfate treatment increase the molecular weight cutoff of polyethylene glycol penetration across murine skin. *Arch Dermatol Res*. 2003; 295:169–174. [PubMed: 12910356]
- Tsai J-C, Sheu H-M, Hung P-L, Cheng C-L. Effect of barrier disruption by acetone treatment on the permeability of compounds with various lipophilicities: Implications for the permeability of compromised skin. *J Pharm Sci*. 2001; 90:1242–1254. [PubMed: 11745777]
- Vogt A, Combadiere B, Hadam S, Stieler KM, Lademann J, Schaefer H, Aufran B, Sterry W, Blume-Peytavi U. 40 nm, but not 750 or 1,500 nm, nanoparticles enter epidermal CD1a+ cells after transcutaneous application on human skin. *J Invest Dermatol*. 2006; 126:1316–1322. [PubMed: 16614727]
- Wahba ZZ, Coogan TP, Rhodes SW, Waalkes MP. Protective effects of selenium on cadmium toxicity in rats: role of altered toxicokinetics and metallothionein. *J Toxicol Environ Health*. 1993; 38(2): 171–182. [PubMed: 8433401]
- Walling MA, Novak JA, Shepard JRE. Quantum dots for live cell and in vivo imaging. *Int J Mol Sci*. 2009; 10:441–491. [PubMed: 19333416]
- Wu J, Liu W, Xue C, Zhou S, Lan F, Bi L, Xu H, Yang X, Zeng F-D. Toxicity and penetration of TiO₂ nanoparticles in hairless mice and porcine skin after subchronic dermal exposure. *Toxicol Lett*. 2009; 191:1–8. [PubMed: 19501137]
- Wu Y, Li X, Steel D, Gammon D, Sham LJ. Coherent optical control of semiconductor quantum dots for quantum information processing. *Physica E: Low-dimensional Systems and Nanostructures*. 2004; 25:242–248.
- Yu WW, Qu L, Guo W, Peng X. Experimental Determination of the Extinction Coefficient of CdTe, CdSe, and CdS Nanocrystals. *Chem Mater*. 2003; 15:2854–2860.
- Zhang LW, Monteiro-Riviere NA. Assessment of quantum dot penetration into intact, tape-stripped, abraded and flexed rat skin. *Skin Pharmacol Appl Skin Physiol*. 2008; 21:166–180.

- Zhang LW, Yu WW, Colvin VL, Monteiro-Riviere NA. Biological interactions of quantum dot nanoparticles in skin and in human epidermal keratinocytes. *Toxicol Appl Pharm.* 2008; 228:200–211.
- Zvyagin AV, Zhao X, Gierden A, Sanchez W, Ross JA, Roberts MS. Imaging of zinc oxide nanoparticle penetration in human skin in vitro and in vivo. *J Biomed Opt.* 2008; 13:064031. [PubMed: 19123677]
- van den Berg JH, Oosterhuis K, Hennink WE, Storm G, van der Aa LJ, Engbersen JFJ, Haanen JBAG, Beijnen JH, Schumacher TN, Nuijen B. Shielding the cationic charge of nanoparticle-formulated dermal DNA vaccines is essential for antigen expression and immunogenicity. *J Control Release.* 2010; 141:234–240. [PubMed: 19751778]
- National Nanotechnology Initiative (NNI). [Accessed 2011] <http://www.nano.gov/>
- [Accessed 2011] The Project on Emerging Nanotechnologies. <http://www.nanotechproject.org/>

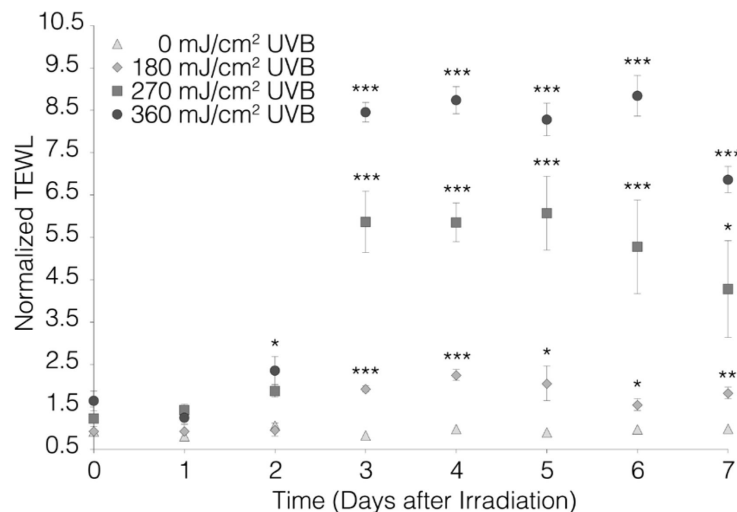


Figure 1. The effect of UVR on skin barrier function as measured by transepidermal water loss (TEWL). Increasing doses of UVR exposure increase the incurred barrier defect (from 0-360 mJ/cm² UVB). A statistically significant increase is observed with all UVB doses with peaks ranging from days 3-6 post-UVR exposure. For this analysis, n=4 mice (2 male and 2 female) were compared to their 0 day time point for each UVB dose using Students paired t-test. Each value is reported as the mean±SEM (*=p<0.05, **=p<0.01, ***=p<0.001).

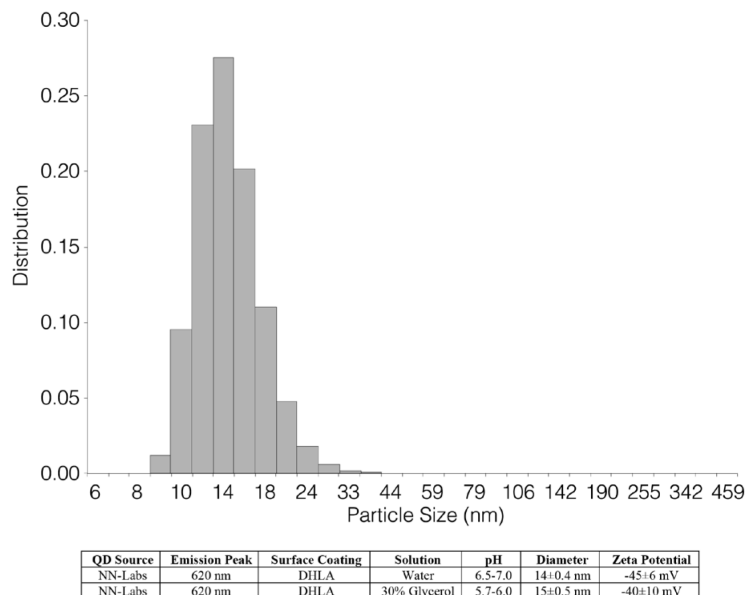


Figure 2. Size and zeta potential measurements for the DHLA encapsulated QDs used in these experiments. DHLA surface coating enables a small stable size in water (depicted) and the 30% glycerol application solution. The zeta potential is strongly negative for each case, and the slight variations observed may be due to differences in pH or viscosity.

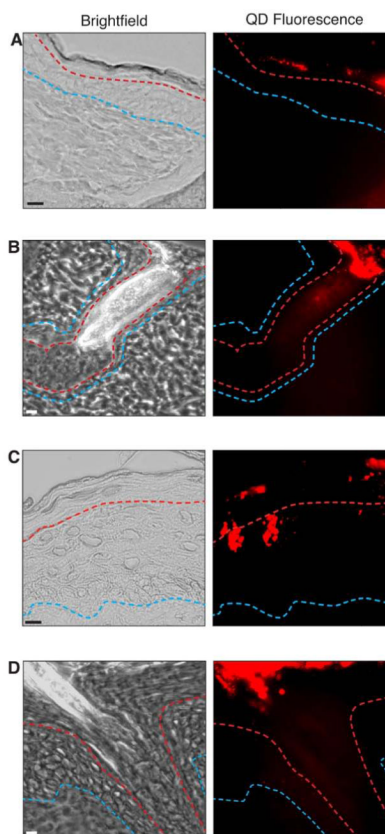


Figure 3.

Collection and penetration trends of QDs with (A) non-UVR irradiated mice and (B) and mice receiving 360 mJ/cm^2 UVB 3.5 days before QD application (C) and (D). Bright field and QD fluorescence images are shown for all conditions with equal fluorescence integration times. Follicular presence of QDs is observable in (B) and (D), with UVR exposure increasing ability of QDs to passively diffuse through the barrier. A clearly observable hyperproliferation response is present when comparing (A) and (C), and there is a notable increase in skin penetration of DHLA coated CdSe/ZnS QDs with UVR exposure. However, the penetration levels after UVR (C) are an extreme example, of which few locations exhibiting such a large amount of diffusion through the stratum corneum barrier were found. Scale bar is $10 \mu\text{m}$.

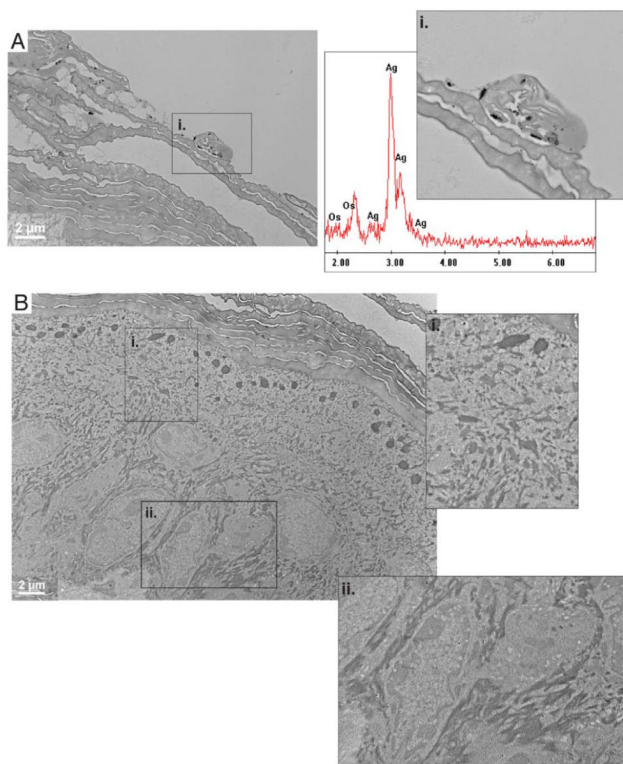


Figure 4. Without UVR irradiation, the collection of QDs is confined mostly to the upper layers of the stratum corneum (A) as observed by TEM. With close examination, the silver enhanced QD morphology can be observed and confirmed by EDAX spectroscopy (i). When lower portions of the stratum corneum and the rest of the epidermis are examined, no evidence of silver enhancement can be observed (B) in the stratum granulosum (i) or the stratum basale (ii).

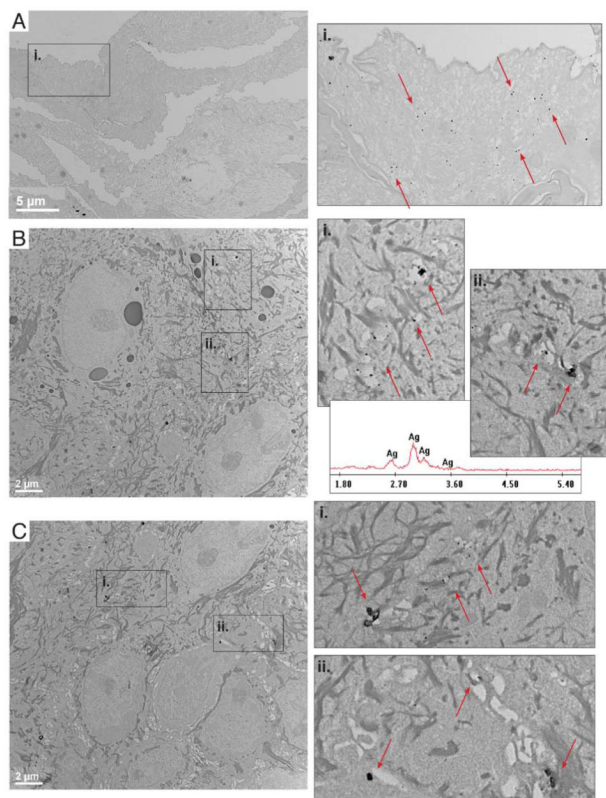


Figure 5.

Exposure to 360 mJ/cm² UVB increases the skin penetration of QDs in a mouse (some QD instances highlighted with red arrows). QD collection in (A,i) and penetration through and between the UVR-damaged outer corneocytes (A) is commonly found. Instances of silver enhanced QDs diffusing through weaknesses in the stratum corneum and epidermis are found in the stratum granulosum (B) with a tendency to move in the cellular boundaries (i, ii). Similar observations can be made in the stratum basale region (C), where long-lasting and highly proliferative basal keratinocytes reside. EDAX confirmation was used to ensure that the particles were silver enhanced QDs.

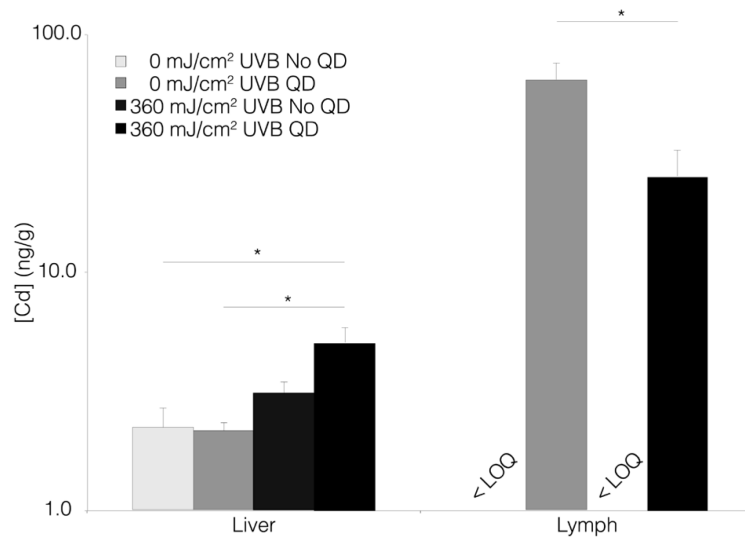


Figure 6.

Atomic absorption spectroscopy of the distal collecting organs to determine tissue Cd concentrations. QD exposure does not induce a statistically significant increase in liver Cd levels for non-irradiated animals. UVR increases liver Cd with and without QD application, and Cd levels were highest in QD treated animals but statistical significance was not achieved (see text). In the lymph nodes, vehicle control treated animals exhibit Cd below the limit of quantification (< LOQ). For QD treated lymph nodes, Cd level decreases after UVR exposure ($p < 0.05$). Each value is reported as the mean \pm SEM ($* = p < 0.05$).

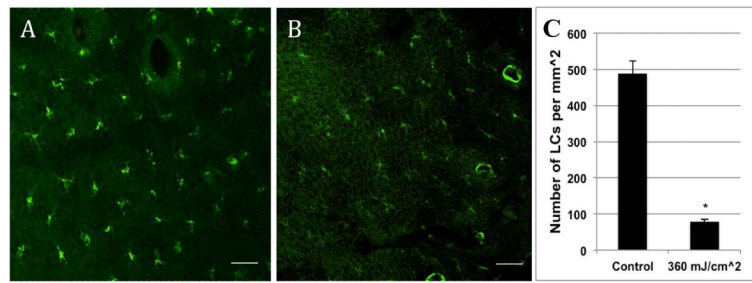


Figure 7.

Confocal microscope images of Langerhans cells (CD207+) in the epidermis of (A) control mouse (no UVR) and (B) mouse 4 days post UVR exposure (360 mJ/cm² UVB).

Quantification of LC cell density (C) indicates there are 478 LCs/mm² in control skin. This decreases ~80% to 79 LCs/mm² in the skin of mice 4 days post UVR (360 mJ/cm² UVB) exposure. Scale bars represent 20 μ m. *p<0.0002

Table 1

Organ mass and total organ Cd for vehicle-only and QD-applied mice (n=5). For non-irradiated and irradiated vehicle-only samples, Cd lymph node presence is below the limit of quantification (< LOQ). Each value is reported as the mean±SEM.

Organ	Radiation Dose	Vehicle		QD	
		Organ Mass (g)	Cd Mass (ng)	Organ Mass (g)	Cd Mass (ng)
Liver	0 mJ/cm ² UVB	1.78±0.13	4.24±0.74	1.78±0.13	3.44±0.33
	360 mJ/cm ² UVB	1.71±0.18	5.72±0.61 ^a	1.65±0.11	7.44±1.17 ^a
Lymph	0 mJ/cm ² UVB	0.03±0.004	< LOQ	0.02±0.003	1.03±0.08
	360 mJ/cm ² UVB	0.02±0.002	< LOQ	0.02±0.003	0.57±0.10 [*]

* significantly different from no UVB group, p = 0.0006;

^a statistically significant main effect of UVB irradiation, p = 0.003.